

# The empirical core-chain model



Boualem Hammouda<sup>a,\*</sup>, Man-Ho Kim<sup>b</sup>

<sup>a</sup> Center for Neutron Research, National Institute of Standards and Technology, Room E 122, Gaithersburg, MD 20899, USA

<sup>b</sup> Advanced Analysis Center, Korea Institute of Science and Technology, Seoul 136-791, South Korea

## ARTICLE INFO

### Article history:

Received 17 July 2017

Received in revised form 6 September 2017

Accepted 27 September 2017

Available online 28 September 2017

## ABSTRACT

Small-angle scattering requires models to analyze the data. A core-chain model has been available to fit data from solutions of core-chain particles. When the core particles are “hard” with well-defined surface, that model has been found to work well and produce characteristic oscillations observed in the data. In the case of “soft” core particles with no well-defined surface and no distinct oscillations in the data, an empirical core-chain model is introduced here. This model includes chain swelling in the grafted polymer chains. It was used to fit small-angle neutron scattering (SANS) data from a dilute solution of core-chain particles in which the core is “soft”. The smooth data trends (no oscillations) are nicely reproduced. Moreover, the radius of gyration of core-chain particles has been worked out and estimated for the measured sample.

Published by Elsevier B.V.

## 1. Introduction

Single-particle form factors are needed to analyze small-angle scattering data from polymers grafted onto the surface of uniform density particles. When the particle fraction is low (in dilute solutions), only the single-particle form factor is needed with small contributions from the inter-particle structure factor.

A molecular model representing the form factor for core-chain particles has been around for some 20 years [1,2]. The main contributions of this model are summarized below. These involve sharp oscillations of the form factor. Polydispersity and the broad instrumental resolution of small-angle neutron scattering (SANS) as well as softness of the core particles damp these oscillations and smear their distinctive features. In such cases, only broad data trends are left from which clues like a radius of gyration and a Porod exponent can be obtained from the Guinier region and the Porod region respectively. A simple empirical core-chain model for the form factor is developed here and compared to the existing molecular core-chain model.

The empirical Guinier-Porod model was introduced for simple particle shapes like spheres, cylinders of lamellae [4]. This model follows the overall trends of scattering data from solutions of particles. It connects up the Guinier part and the Porod part seamlessly and yields a radius of gyration and a Porod exponent. The same idea is used here to derive the empirical form factor for soft core-chain particles.

Since the radius of gyration of a core-chain particle has not been worked out, it is derived here as well.

## 2. The original core-chain model

The original core-chain model [1,2] is reviewed here. Consider polymer chains grafted onto a spherical particle. The uniform core is denoted by index *c* and the grafted polymer is denoted by index *p*. The cross section for a dilute solution of uniform core-grafted polymer chain model  $d\Sigma_s(Q)/d\Omega$  has the following contributions: core-core (Term1), polymer-polymer within the same chain (Term2), core-polymer chain cross product (Term3) and polymer-polymer correlations across two different grafted chains (Term4).

Following the approach of Pedersen [1,2], these contributions are given by:

$$\begin{aligned} \frac{d\Sigma_s(Q)}{d\Omega} &= \{\text{Term1} + \text{Term2} + \text{Term3} + \text{Term4}\} \\ \text{Term1} &= \Delta\rho_c^2 V_c^2 P_c(QR) \\ \text{Term2} &= \Delta\rho_p^2 V_p^2 N_p P_p(QR_g) \\ \text{Term3} &= 2\Delta\rho_c V_c F_c(QR) E_c(QR) \Delta\rho_p V_p N_p F_p(QR_g) \\ \text{Term4} &= \Delta\rho_p^2 N_p (N_p - 1) V_p^2 F_p^2(QR_g) E_c^2(QR) \end{aligned} \quad (1)$$

The scattering length density difference for the core part  $\Delta\rho_c$  and for the chain part  $\Delta\rho_p$  have been defined along with the core volume  $V_c$  and (chain) monomer volume  $V_p$ .  $N_p$  is the number of grafted polymer molecules on each core particle.  $Q$  is the scattering variable.

\* Corresponding author.

E-mail address: [hammouda@nist.gov](mailto:hammouda@nist.gov) (B. Hammouda).

The various form factors ( $P_c$  and  $P_p$ ), form factor amplitudes ( $F_c$  and  $F_p$ ), and propagators ( $E_c$  and  $E_p$ ), for the spherical core (of radius  $R$ ) and grafted chain parts are given by;

$$\begin{aligned}
 P_c(QR) &= (F_c(QR))^2 = \left(\frac{3j_1(QR)}{QR}\right)^2 \\
 P_p(QR_g) &= \frac{2}{(QR_g)^2} \left[ \exp(-Q^2R_g^2) - 1 + Q^2R_g^2 \right] \\
 F_c(QR) &= \left(\frac{3j_1(QR)}{QR}\right) \\
 F_p(QR_g) &= \left(\frac{1 - \exp(-Q^2R_g^2)}{Q^2R_g^2}\right) \\
 E_c(QR) &= \left(\frac{\sin|QR|}{QR}\right)
 \end{aligned}
 \tag{2}$$

Here  $j_1(QR)$  is the spherical Bessel function of order 1 that produces oscillations for hard core particles. The original approach was worked out for Gaussian chains (that follow random statistics) and is generalized here to account for grafted chain with excluded volume [3] as follows:

$$\begin{aligned}
 P_p(Q) &= \frac{1}{\nu U^{1/2\nu}} \gamma\left(\frac{1}{2\nu}, U\right) - \frac{1}{\nu U^{1/\nu}} \gamma\left(\frac{1}{\nu}, U\right) \\
 F_p(Q) &= \frac{1}{2\nu U^{1/2\nu}} \gamma(1/2\nu, U)
 \end{aligned}
 \tag{3}$$

Here,  $\gamma(x,U)$  is the incomplete gamma function and  $U$  has been defined as:

$$U = \frac{Q^2 a^2 n^{2\nu}}{6} = \frac{Q^2 R_g^2 2\nu + 12\nu + 2}{6}
 \tag{4}$$

Moreover,  $a$  is the statistical segment length,  $n$  is the degree of polymerization of the grafted polymer chains,  $\nu$  is the excluded volume parameter and  $R_g$  is the radius of gyration.

The cross section for a dilute solution of core-chain particles sums up all four contributions:

$$\begin{aligned}
 \frac{d\Sigma_s(Q)}{d\Omega} &= \left\{ \Delta\rho_c^2 V_c^2 P_c(QR) + \Delta\rho_p^2 V_p^2 N_p P_p(QR_g) \right. \\
 &\quad + 2 \Delta\rho_c V_c F_c(QR) E_c(QR) \Delta\rho_p V_p N_p F_p(QR_g) \\
 &\quad \left. + \Delta\rho_p^2 N_p (N_p - 1) V_p^2 F_p^2(QR_g) E_c^2(QR) \right\}
 \end{aligned}
 \tag{5}$$

### 3. The empirical core-chain model

Following the approach taken in deriving the Guinier-Porod model [4], an empirical core-chain model is derived here for cases with soft core particles; i.e., where there are no oscillations in the data. The chain part remains as before but the core contributions simplify as follows. The Guinier part for the core form factor is given by  $P_c(Q) = \exp[-Q^2R^2/5]$ . The form factor amplitude is the square root of the form factor and is given by  $F_c(Q) = \exp[-Q^2R^2/10]$ .

For the core part factors  $P_c$ ,  $F_c$  and  $E_c$ , the idea is to connect up these functions and their derivatives at transition points ( $Q_1$  and  $Q_2$ ) to yield.

$$\begin{aligned}
 P_c(Q) &= \exp\left[-\frac{Q^2R^2}{5}\right] \text{ for } Q \leq Q_1 \\
 F_c(Q) &= \exp\left[-\frac{Q^2R^2}{10}\right] \text{ for } Q \leq Q_1 \\
 P_c(Q) &= \frac{P_1}{Q^m} \text{ for } Q \geq Q_1 \\
 F_c(Q) &= \frac{P_1}{Q^{m/2}} \text{ for } Q \geq Q_1.
 \end{aligned}
 \tag{6}$$

Here  $m$  is a Porod exponent. The transition point for the core form factor and form factor amplitude (horizontal scale) is given by:

$$Q_1 = \frac{1}{R} \sqrt{\frac{5m}{2}}
 \tag{7}$$

The connection between the Guinier and Porod scale factors (vertical scale) is given by:

$$P_1 = G_1 \exp\left[-\frac{Q_1^2R^2}{5}\right] Q_1^m
 \tag{8}$$

The core propagator has a different transition point at  $Q_2$ .

$$\begin{aligned}
 E_c(Q) &= \exp\left[-\frac{Q^2R^2}{6}\right] \text{ for } Q \leq Q_2 \\
 E_c(Q) &= \frac{P_2}{Q^{m/4}} \text{ for } Q \geq Q_2 \\
 Q_2 &= \frac{1}{R} \sqrt{\frac{3m}{4}} \\
 P_2 &= \exp\left[-\frac{Q_2^2R^2}{6}\right] Q_2^{m/4}.
 \end{aligned}
 \tag{9}$$

Since the radius of gyration for core-chain particles had not been worked out before, it is included next.

### 4. Radius of gyration for the core-chain particle

The radius of gyration  $R_{g\text{core-chain}}$  for a core-chain particle is worked out here. It has four contributions just like the form factor does.

$$\begin{aligned}
 I(Q) &= K \exp\left[-\frac{Q^2R_g^2}{3}\right] \quad K \text{ is the "machine" constant} \\
 R_{g\text{core-chain}}^2 &= -3 \left[ \frac{\partial \ln[I(Q)]}{\partial Q^2} \right]_{Q=0} = -3 \left[ \frac{\partial I(Q)}{\partial Q^2} \frac{1}{I(Q)} \right]_{Q=0}
 \end{aligned}
 \tag{10}$$

The various contributions follow.

$$\begin{aligned}
 \left[ \frac{\partial P_c(Q)}{\partial Q^2} \right]_{Q=0} &= -\frac{R^2}{5} \\
 \left[ \frac{\partial P_p(Q)}{\partial Q^2} \right]_{Q=0} &= -\frac{R_g^2}{3} \\
 \left[ \frac{\partial F_c(Q) E_c(Q) F_p(Q)}{\partial Q^2} \right]_{Q=0} &= \left[ \frac{\partial F_c(Q)}{\partial Q^2} E_c(Q) F_p(Q) + F_c(Q) \frac{\partial E_c(Q)}{\partial Q^2} F_p(Q) \right. \\
 &\quad \left. + F_c(Q) E_c(Q) \frac{\partial F_p(Q)}{\partial Q^2} \right]_{Q=0} \\
 \left[ \frac{\partial F_c(Q) E_c(Q) F_p(Q)}{\partial Q^2} \right]_{Q=0} &= -\frac{R}{10} - \frac{R^2}{6} - \frac{R_g^2}{2} \\
 \left[ \frac{\partial E_c^2(Q) F_p^2(Q)}{\partial Q^2} \right]_{Q=0} &= \left[ \frac{2\partial E_c(Q)}{\partial Q^2} F_p^2(Q) + E_c^2(Q) \frac{2\partial F_p(Q)}{\partial Q^2} \right]_{Q=0} = -\frac{R^2}{3} - R_g^2
 \end{aligned}
 \tag{11}$$

The radius of gyration squared gathers all contribution to yield the final result as follows.

$$R_{\text{gcore-chain}}^2 = \frac{\text{Num}}{\text{Den}}$$

$$\text{Num} = \left\{ \Delta\rho_c^2 V_c^2 \frac{3}{5} R^2 + \Delta\rho_p^2 V_p^2 N_p R_g^2 + 2 \Delta\rho_c V_c \Delta\rho_p V_p N_p \left[ \frac{3}{10} R^2 + \frac{1}{2} R^2 + \frac{3}{2} R_g^2 \right] + \Delta\rho_p^2 N_p (N_p - 1) V_p^2 \left[ R^2 + 3 R_g^2 \right] \right\}$$

$$\text{Den} = \left\{ \Delta\rho_c^2 V_c^2 + \Delta\rho_p^2 V_p^2 N_p + 2 \Delta\rho_c V_c \Delta\rho_p V_p N_p + \Delta\rho_p^2 N_p (N_p - 1) V_p^2 \right\} \quad (12)$$

Note that the radius of gyration of the core-chain (compound) particle depends on the scattering length densities. This is counterintuitive and is tantamount to saying that the size of a compound particle depends on its “color”. This conclusion, however, has been verified and is reliable. In this calculation, the radius of gyration of one grafted polymer chain has been used as  $R_g^2 = N_m a^{2\nu} / (2\nu + 1)(2\nu + 2)$ .

The limit of a pure core particle is recovered by setting  $N_p = 0$ ,  $V_p = 0$ , in which case one recovers  $R_{\text{gcore-chain}}^2 = 3R^2/5$ . Similarly, the limit of pure polymer is also recovered by setting  $R_c = 0$  (and therefore  $V_c = 0$ ), and the result is as follows:

$$R_{\text{gcore-chain}}^2 = \frac{\left\{ R_g^2 + (N_p - 1) \left[ 3R_g^2 \right] \right\}}{1 + (N_p - 1)} \quad (13)$$

Note that this limit covers star-branched polymers as well. Setting additionally  $N_p = 1$  yields  $R_{\text{gcore-chain}}^2 = R_g^2$  which is the right result for a homopolymer (single branch). When  $N_p = 2$ ,  $R_{\text{gcore-chain}}^2 = 2R_g^2 = na^2/3$  as it should. Here, in the limit of Gaussian chains ( $\nu = 0.5$ ) the radius of gyration of a single branch (squared) is given by  $R_g^2 = na^2/6$ .

## 5. Plot of the core-chain and the empirical core-chain models

A figure compares the core-chain and the empirical core-chain models (Fig. 3). Parameters used are:

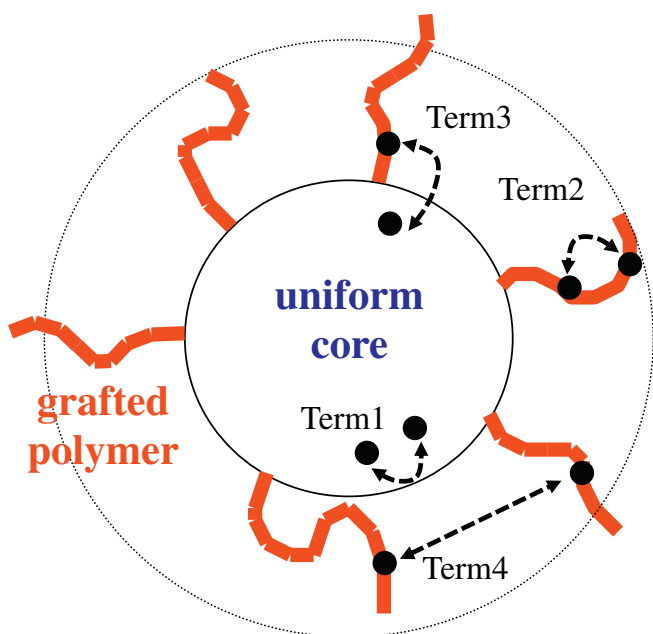


Fig. 1. Schematic representation of the uniform core-grafted polymer chain showing the four types of correlations.

core radius  $R = 50 \text{ \AA}$ , number of grafted chains  $N_p = 100$ , number of monomers per grafted chain  $N_m = 100$ , monomer volume  $v_m = 100 \text{ \AA}^3$ , segment length  $a = 5 \text{ \AA}$  and excluded volume parameter  $\nu = 0.5$ . The scattering length densities used are  $\rho_c = 4 * 10^{-6} \text{ \AA}^{-2}$  for the core,  $\rho_p = 5 * 10^{-6} \text{ \AA}^{-2}$  for the grafted chains and  $\rho_s = 6 * 10^{-6} \text{ \AA}^{-2}$  for the solvent.

Oftentimes, to analyze scattering data, two models representing the main features observed in the data are added up. In the present case, the two main contributions are from the core and from the grafted chains. This neglects the cross terms like in our case Term3 and Term4 (see Figs. 1 and 2). In order to assess the contribution of these cross terms, Fig. 4 is plotted. This figure shows that the cross terms are not negligible in general. The different vertical scales in the two cases are due to the different contrast factors in the various terms (Term1 to Term4). In order to compare the Q-dependences of the two cases (“with” and “without the cross terms”), the form factor without the cross terms is rescaled. This clearly shows different Q-dependences implying that the cross terms should be taken into account in models used to fit scattering data.

## 6. Fit to SANS data

Small-angle neutron scattering (SANS) data have been acquired from a dilute solution of core-chain particles. The soft core is formed of a crosslinked ethylene glycol dimethylacrylate (EGDMA) nanogel upon which PMMA chains ( $M_w = 17 \text{ kg/mol}$ ) are grafted. Short P3HT chains ( $M_w = 4 \text{ kg/mol}$ ) are covalently bonded at the end of the grafted PMMA chains. The overall mass fraction of the core-chain particles is 0.5% and the solvent used is deuterated toluene. Measurements were made at  $50 \text{ }^\circ\text{C}$ , temperature at which P3HT is amorphous (sample named MHK-20\_50C). SANS data were taken at three standard configurations yielding a wide reliable Q-range. Reduced SANS data were fit using the empirical core-chain model for the form factor.

Looking at the trends of the data (Fig. 5), one would be tempted to fit the low-Q ( $Q < 0.04 \text{ \AA}^{-1}$ ) data to the form factor for core and the high-Q data ( $Q > 0.04 \text{ \AA}^{-1}$ ) to the chain form factor. The previous discussion shows, however, that this would account for the first two terms only (Term1 + Term2) and would neglect the cross terms (Term3 + Term4) completely. Note that the Q-independent incoherent background (from hydrogen scattering) has been subtracted from the data. Since the data trends are not characterized by oscillations, the empirical core-chain model fits the data well.

The resulting fit parameters are as follows (Fig. 5): core radius  $R = 96.6 \text{ \AA}$ , number of grafted chains  $N_p = 4$ , number of monomers per grafted chain  $N_m = 115$ , monomer volume  $v_m = 163 \text{ \AA}^3$ , segment length  $a = 8.7 \text{ \AA}$  and excluded volume parameter  $\nu = 0.81$ . The scattering length densities used are  $\rho_c = 5.4 * 10^{-6} \text{ \AA}^{-2}$  for the core,  $\rho_p = 9.4 * 10^{-7} \text{ \AA}^{-2}$  for the grafted chains and  $\rho_s = 5.5 * 10^{-6} \text{ \AA}^{-2}$  for the solvent. Note that the known parameters have been kept constant to help the fit process. A scale factor of  $\text{Scale} = 1 * 10^{-16}$  has been used to convert the cross section from the  $\text{\AA}^{-1}$  scale (natural variable in the model) to the  $\text{cm}^{-1}$  scale (measured absolute cross section). These fitting parameters correspond to one standard deviation (68% confidence level).

Given the obtained fit parameters characterizing the sample used (MHK-20\_50C), the radius of gyration can be calculated as follows. The radius of gyration squared for the core-chain particle contains the four contributions (core-core, chain-chain on the same chain, core-chain and chain-chain on two different chains as described in Eq. (12)) added in quadrature as  $R_{\text{gcore-chain}}^2 = 3076 + 18327 + 250300 + 168094 = 439796 \text{ \AA}^2$  thereby yielding a core-chain particle radius of gyration of  $R_{\text{gcore-chain}} = 663 \text{ \AA}$ .

## 7. The Guinier-Porod model literature

The Guinier-Porod model [4] was introduced to calculate the form factor for spherically symmetric (compact) particles. The

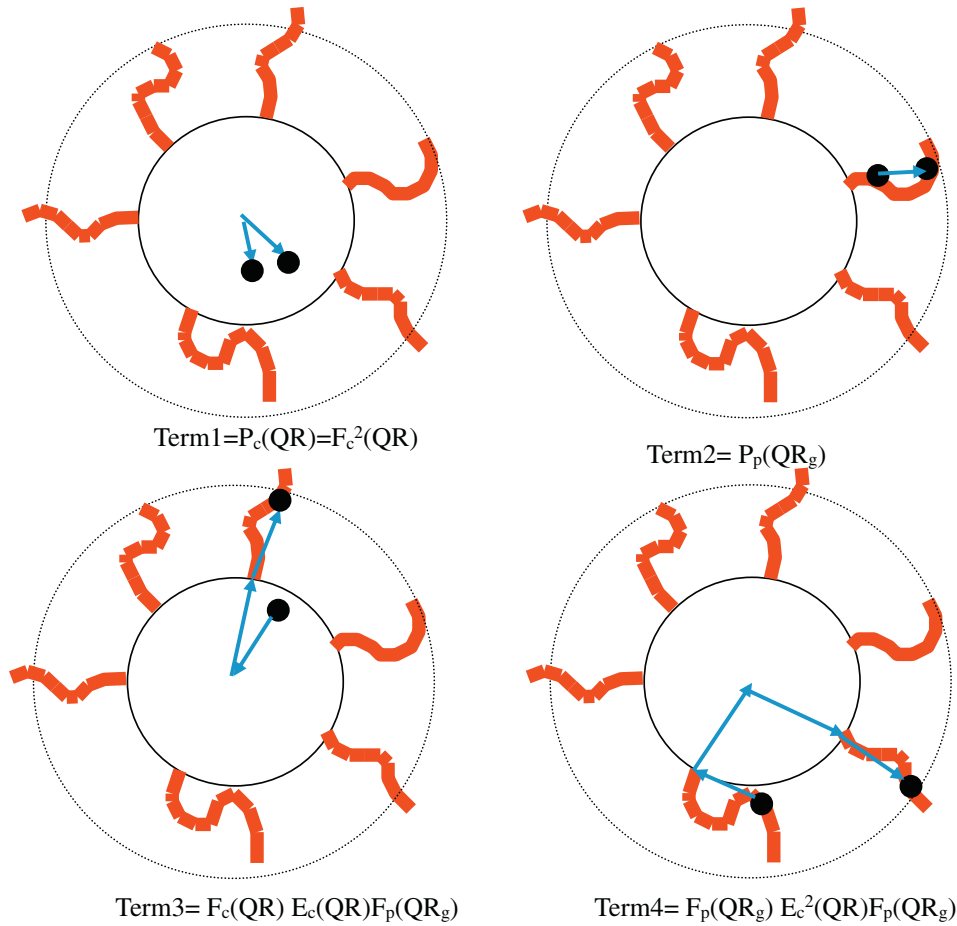


Fig. 2. Breaking down the contributions to the four correlation terms.

generalized Guinier-Porod model broadened the application of this model to elongated particles. The Guinier-Porod model was compared to the Beaucage model [5] also referred as unified model. A

number of investigations using the Guinier-Porod model are described in this section.

The generalized Guinier-Model was used to fit SANS data from pluronic micelles [6] at various temperatures and therefore of various shapes (spherical, cylindrical and lamellar). This single empirical

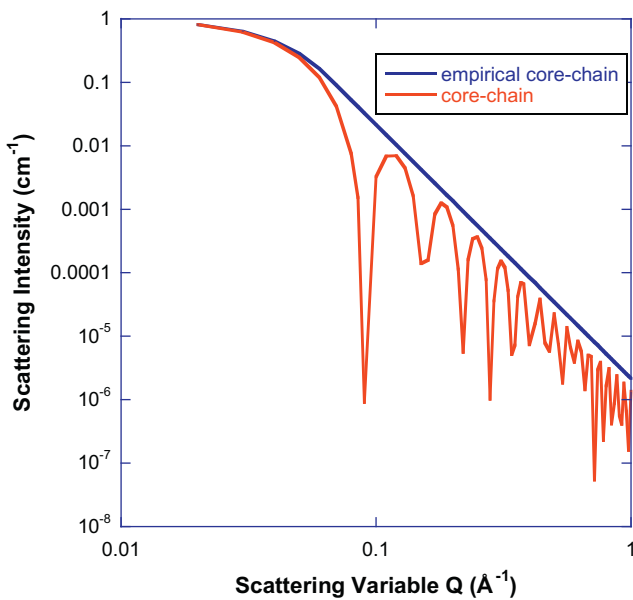


Fig. 3. Variation of the normalized core-chain form factor  $P(Q)$  as function of  $Q$  for the original core-chain model (oscillating case) and the empirical core-chain model (smoothened case). The former applies to hard core particles while the latter applies to soft core particles.

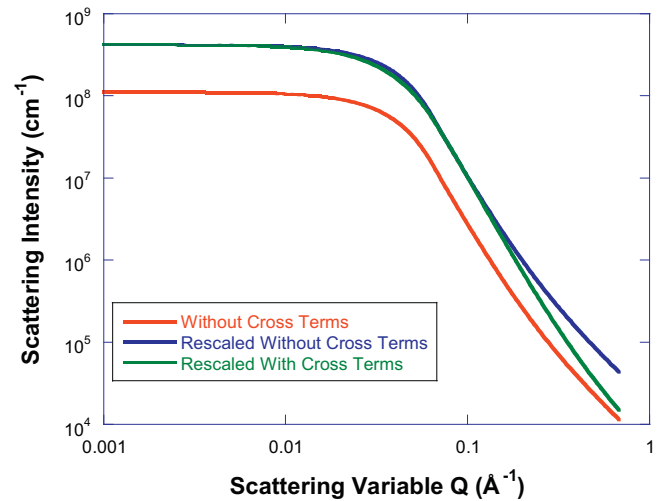


Fig. 4. Contribution of all four terms (Term1 + Term2 + Term3 + Term4); i.e., “with the cross terms” of the form factor as compared to contribution of the first two terms (Term1 + Term2) only, i.e., “without the cross terms” (Term3 + Term4). The “without cross terms” curve has been rescaled to coincide with the “with cross terms” result (at low- $Q$ ) in order to compare their  $Q$ -dependence.

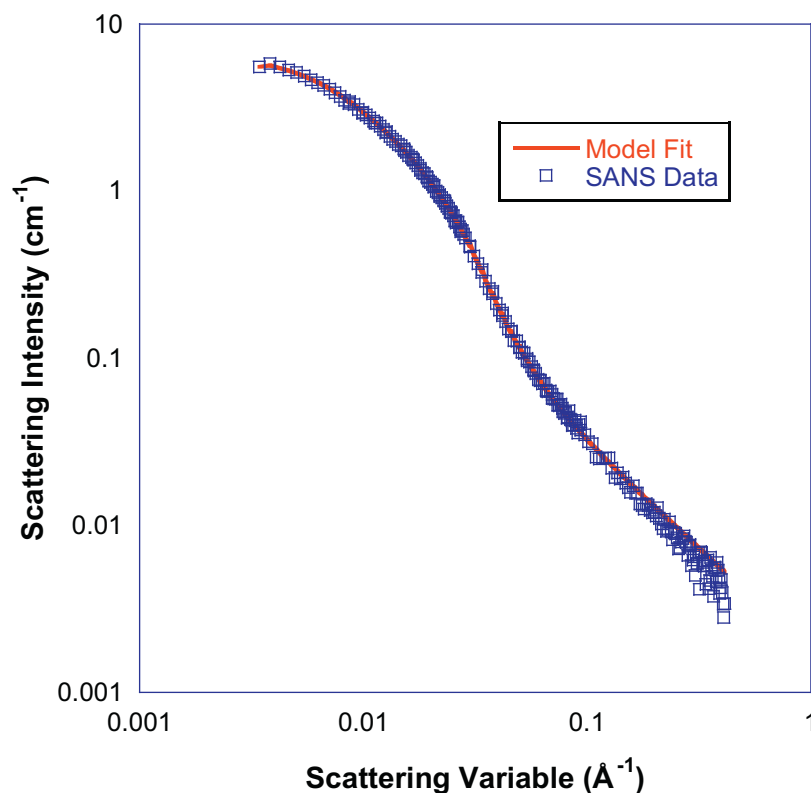


Fig. 5. Comparison of the SANS data to the empirical core-chain model fit.

model substituted for the use of three molecular models (for sphere, cylinder and lamella) as well as condition in-between.

The interesting phase transitions observed by raising sample temperature for P85 micelles were investigated when pressure was raised as well [7]. Note that at high temperature (higher than the boiling temperature of water), a new phase was observed. This was possible by pressurizing the sample.

The microstructure network of bulk (Bi,Sb)<sub>2</sub>Te<sub>3</sub> synthesized using two different processes (melt-spinning and spark-plasma-sintering) was investigated by SANS [8]. The generalized Guinier-Porod model was used to identify and characterize the lamellar structure and lamellar surface roughness.

The SANS technique was used to investigate the nanostructure of bottlebrush polymers in solution. The generalized Guinier-Porod model was used to obtain the radius of gyration of the bottlebrush macromolecules [9]. Variation of the backbone or the side-chains yielded different sizes. A sphere-to-cylinder transition was observed with increasing backbone size.

SANS investigations were performed on similar bottlebrush polymers but now varying side chain length and end group structure [10]. The generalized Guinier-Porod model was here also used to obtain macromolecular dimensions and solution mixing-demixing characteristics.

The bottlebrush polymers project was pursued further by focusing on scaling laws of the radius of gyration with varying molecular weight of the backbone and/or side chains [11]. Side chains were found to be weakly stretched (the end-to-end distance varies with degree of polymerization  $N$  as  $N^{0.55}$  while the overall bottlebrush increases in size proportional to  $N^{0.77}$ ). This demonstrates that the bottlebrush backbone is not fully extended and that both backbone and side chains have significant conformational flexibility in solution.

The nanostructure of self-assembled water/polyalphaolefin nanoemulsion fluids was investigated using SANS and correlated to the thermophysical properties like the thermal conductivity [12]. The generalized Guinier-Porod model yielded the variation of the nanodroplet size and shapes its variation with increasing water fraction. For instance, the

thermal conductivity was found to vary linearly with water fraction but appears to be insensitive to nanostructural changes.

The correlation between the morphology of catalyst supports,  $\gamma$ -alumina ( $\gamma$ -Al<sub>2</sub>O<sub>3</sub>), and their activity in a Pt/alumina system was investigated using the generalized Guinier-Porod model [13]. The shape and aggregation of  $\gamma$ -alumina were found to affect catalytic performance on a nano/micro scale.

The Guinier-Porod model has proven to be useful for the analysis of small-angle scattering data. This includes SANS and SAXS (small-angle X-ray scattering). It has been used to analyze soft matter as well as hard matter. Papers scanning the entire spectrum are referenced here [14–53].

## 8. Summary and discussion

The original core-chain model has been used extensively [1,2]. That model has been extended here to accommodate excluded volume effects when the grafted chains are swollen. Scattering data trends point to non-negligible swelling (good solvent) that shows up as a high- $Q$  Porod exponent less than 2 (non-ideal chains). In cases where SANS data are not characterized by sharp oscillations; i.e., when the core particles are not hard (with no well-defined surface) an empirical core-chain model has been presented for the form factor. This model reproduces the appropriate limits such as the pure core particle limit (with no grafted chains) and the coreless chains limit (with no core particle). In this last case, one can reproduce the simple case of a homopolymer as well as the case of star-branched polymers. Note that pure polymers are “mean field” scatterers devoid of sharp oscillations. The empirical core-chain model introduced here is reminiscent of the Guinier-Porod model [4] that was introduced a few years back. The Guinier-Porod model is found to be useful. Citations of the original paper are increasing nicely. The Guinier-Porod model applies to globular scattering particles and to anisotropic ones (like cylinders and lamellae) as well as to structures in-between.

In order to analyze scattering data, it is common practice to use models that reproduce the overall trends in the data. If the data have two main distinct features, two models are usually added up to fit the

data. This approach neglects the cross terms. Using the empirical core-chain model, contribution of the cross terms has been shown to be non-negligible. These change the  $Q$ -dependence of the model noticeably.

Fit of the empirical core-chain model to SANS data from a dilute solution of core-chain particles yielded reasonable results. The scattering data were devoid of oscillations owing to the softness of the particle core. This model was appropriate to fit the smooth features of this data type. Note that the core-chain model introduced here applies to dilute solutions only since no inter-particle structure factor has been discussed.

Moreover, the radius of gyration for core-chain particles has been worked out in this paper as well and applied to estimate it for the measured sample.

## Acknowledgements

We thank Dr. K.Y. Baek (Korea Institute of Science and Technology) for providing a test sample. The identification of commercial products does not imply endorsement by the National Institute of Standards and Technology nor does it imply that these are the best for the purpose. The SANS part of this work is based upon activities supported in part by the US National Science Foundation under Agreement No. DMR-1508249.

## References

- [1] J.S. Pedersen, M.C. Gerstenberg, Scattering form factor of block copolymer micelles, *Macromolecules* 29 (1996) 1963–1965.
- [2] J.S. Pedersen, M.C. Gerstenberg, The structure of P85 Pluronic copolymer micelles determined by SANS, *Colloids Surf. A Physicochem. Eng. Asp.* 213 (2003) 175–187.
- [3] B. Hammouda, SANS from homogeneous polymer systems: a unified overview, *Adv. Polym. Sci.* 106 (1993) 87–133.
- [4] B. Hammouda, A new Guinier–Porod model, *J. Appl. Crystallogr.* 43 (2010) 716–719.
- [5] B. Hammouda, Analysis of the Beaucage model, *J. Appl. Crystallogr.* 43 (2010) 1474–1478.
- [6] B. Hammouda, SANS from Pluronic P85 in d-water, *Eur. Polym. J.* 46 (2010) 2275–2281.
- [7] B. Hammouda, SANS from P85/d-water under pressure, *Langmuir* 26 (2010) 6625–6629.
- [8] W. Xie, D.A. Hitchcock, H.J. Kang, J. He, X. Tang, M. Laver, B. Hammouda, The microstructure network and thermoelectric properties of bulk (Bi,Sb)2Te3, *Appl. Phys. Lett.* 101 (2012) 113902–1–113902–4.
- [9] S. Pesek, X. Li, B. Hammouda, R. Verduzco, Synthesis and conformational analysis of bottlebrush polymers by SANS, *Macromolecules* 46 (2013) 6998–7005.
- [10] X. Li, H. Shamsijazeyi, S. Pesek, A. Agrawal, B. Hammouda, R. Verduzco, P.N.I.P.A.A.M. Thermoresponsive, Bottlebrush polymers with tailored side-chain length and end-group structure, *Soft Matter* 10 (2014) 2008–2015.
- [11] S. Pesek, Q. Xiang, B. Hammouda, R. Verduzco, SANS analysis of bottlebrush backbone and side chain flexibility, *J. Polym. Sci. Polym. Phys.* 55 (2017) 104–111.
- [12] J. Xu, B. Hammouda, F. Cao, B. Yang, Experimental Study of thermophysical properties and nanostructure of self-assembled water/polyalphaolefin nanoemulsion fluids, *Adv. Mech. Eng.* 7 (2015) 1–8.
- [13] S.H. Kim, S. Han, H. Ha, J.Y. Bryun, M.-H. Kim, Support-shape dependent catalytic activity in Pt/alumina systems using ultra-small (USANS) and small-angle neutron scattering (SANS), *Catal. Today* 260 (2016) 46–54.
- [14] H. Luo, M. Szymusiak, E. Alexandra, G. Lye, L. Lock, H. Cui, Y. Liu, M. Herrera-Alonso, Solute-triggered morphological transitions of an amphiphilic heterografted brush copolymer as a single-molecule drug carrier, *Macromolecules* 50 (2017) 2201–2206.
- [15] B.J. Rohde, K.M. Le, R. Krishnamoorti, M.L. Robertson, Thermoset blends of an epoxy resin and polydicyclopentadiene, *Macromolecules* 49 (2016) 8960–8970.
- [16] S. Kishore, S. Srivastava, S.R. Bhatia, Microstructure of colloid-polymer mixtures containing charged colloidal disks and weakly-adsorbing polymers, *Polymer* 105 (2016) 461–471.
- [17] T. Li, A.J. Senesi, B. Lee, Small angle X-ray scattering for nanoparticle research, *Chem. Rev.* 116 (2016) 11128–11180.
- [18] T.G. Barclay, H. Rajapaksha, A. Thilagam, G. Qiana, M. Ginic-Markovica, P.D. Cooper, A. Gerson, N. Petrovsky, Physical characterization and in silico modeling of inulin polymer conformation during vaccine adjuvant particle formation, *Carbohydr. Polym.* 143 (2016) 108–115.
- [19] H. Kurig, M. Russina, I. Tallo, M. Siebenbürger, T. Romann, E. Lust, The suitability of infinite slit-shaped pore model to describe the pores in highly porous carbon materials, *Carbon* 100 (2016) 617–624.
- [20] C.J. Gommès, G. Prieto, P.E. de Jongh, Small-angle scattering analysis of empty or loaded hierarchical porous materials, *J. Phys. Chem. C* 120 (2016) 1488–1506.
- [21] C.D. Umeasiegbu, V. Balakotaiah, R. Krishnamoorti, pH-Induced re-entrant microstructural transitions in cationic surfactant-hydrotrope mixtures, *Langmuir* 32 (2016) 655–666.
- [22] D. Naumenko, L. Stolzer, A.S. Quick, D. Abt, M. Wegener, C. Barner-Kowollik, S. Dal Zilio, B. Marmiroli, H. Amenitsch, L. Fruk, M. Lazzarino, Design of broadband SERS substrates by the laser-induced aggregation of gold nanoparticles, *J. Mater. Chem. C* 4 (2016) 6152–6159.
- [23] J.L. Whittaker, N.K. Dutta, R. Knott, G. McPhee, N.H. Voelcker, C. Elvin, A. Hill, N.R. Choudhury, Tunable thermoresponsiveness of resilin via coassembly with rigid biopolymers, *Langmuir* 31 (2015) 8882–8891.
- [24] P.M. de Molina, S. Lad, M.E. Helgeson, Heterogeneity and its influence on the properties of difunctional poly(ethylene glycol) hydrogels: structure and mechanics, *Macromolecules* 48 (2015) 5402–5411.
- [25] M. Martínez-Sanz, M.J. Gidley, E.P. Gilbert, Application of X-ray and neutron small angle scattering techniques to study the hierarchical structure of plant cell walls: a review, *Carbohydr. Polym.* 125 (2015) 120–134.
- [26] S.H.S. Koshari, N.J. Wagner, A.M. Lenhoff, Characterization of lysozyme adsorption in cellulosic chromatographic materials using small-angle neutron scattering, *J. Chromatogr. A* 1399 (2015) 45–52.
- [27] Z. Chen, P.A. FitzGerald, G.G. Warr, R. Atkin, Conformation of poly(ethylene oxide) dissolved in the solvate ionic liquid [Li(G4)]TFSI, *Phys. Chem. Chem. Phys.* 17 (2015) 14872–14878.
- [28] M. Romero, H. Pardo, R. Faccio, M.A. Tumelero, C. Campos, J. PlaCid, A.A. Castiglioni, A.W. Pasa, Momburu, Interphase and magnetotransport of LSMO-PMMA nanocomposites obtained by a sonochemical method, *J. Magn. Magn. Mater.* 382 (2015) 342–348.
- [29] M. Girod, S. Vogel, W. Szczerba, A.F. Thünemann, How temperature determines formation of maghemite nanoparticles, *J. Magn. Magn. Mater.* 380 (2015) 163–167.
- [30] B. Soptei, J. Mihaly, I.Cs. Szgyarto, A. Wach, C. Nemetha, I. Bertoti, Z. May, P. Baranyai, I.E. Sajo, A. Bota, The supramolecular chemistry of gold and l-cysteine: Formation of photoluminescent, orange-emitting assemblies with multilayer structure, *Colloids Surf. A Physicochem. Eng. Asp.* 470 (2015) 8–14.
- [31] H. Zhang, X. Liu, S. Feng, W. Wang, K. Schmidt-Rohr, M. Akinc, M. Nilsen-Hamilton, D. Vaknin, S. Mallapragada, Morphological transformations in the magnetite biomimetic protein Mms6 in iron solutions: a small-angle X-ray scattering study, *Langmuir* 31 (2015) 2818–2825.
- [32] M. Romero, R. Faccio, H. Pardo, M.A. Tumelero, A.A. Pasa, Alvaro W. Momburu, Microstructural and magnetotransport studies of novel manganese–sebacic acid nanocomposites prepared at low temperature, *J. Magn. Magn. Mater.* 377 (2015) 490–495.
- [33] D. Alaimo, D.H. Merino, B. Grignard, W. Bras, C. Jeeroome, A. Debuigne, C.J. Gommès, Small-angle X-ray scattering insights into the architecture-dependent emulsifying properties of amphiphilic copolymers in supercritical carbon dioxide, *J. Phys. Chem. B* 119 (2015) 1706–1716.
- [34] D. Molodenskiy, E. Shirshin, T. Tikhonova, A. Gruzinov, G. Peters, F. Spinuzzi, Thermally induced conformational changes and protein–protein interactions of bovine serum albumin in aqueous solution under different pH and ionic strengths as revealed by SAXS measurements, *Phys. Chem. Chem. Phys.* 19 (2017) 17143–17155.
- [35] L.N. Nagy, J. Mihaly, A. Polyak, B. Debreczeni, B. Csaszar, I.Cs. Szgyarto, A. Wach, Zs. Czegeny, E. Jakab, Sz. Klebert, E. Drotar, G. Dabasi, A. Bota, L. Balogh, E. Kiss, Inherently fluorescent and porous zirconia colloids: preparation, characterization and drug adsorption studies, *J. Mater. Chem. B* 3 (2015) 7529–7537.
- [36] M. Romero, R. Faccio, J. Martínez, H. Pardo, B. Montenegro, C. Campos Pla Cid, A.A. Pasa, A.W. Momburu, Effect of lanthanide on the microstructure and structure of LnMn0.5Fe0.5O3 nanoparticles with Ln/La, Pr, Nd, Sm and Gd prepared by the polymer precursor method, *J. Solid State Chem.* 271 (2015) 325–333.
- [37] F. Peyronel, B. Quinn, A.G. Marangoni, D.A. Pink, Ultra small angle X-ray scattering for pure tristearin and tripalmitin: model predictions and experimental results, *Food Biophys.* 9 (2014) 304–313.
- [38] S.A. Jamieson, K.W.K. Tong, W.A. Hamilton, L. He, M. James, P. Thordarson, Small angle neutron scattering (SANS) studies on the structural evolution of pyromellitimide self-assembled gels, *Langmuir* 30 (2014) 13987–13993.
- [39] F. Peyronel, B. Quinn, A.G. Marangoni, D.A. Pink, Ultra small-angle X-ray scattering in complex mixtures of triacylglycerols, *J. Phys. Condens. Matter* 26 (2014) 464110.
- [40] B. Quinn, F. Peyronel, T. Gordon, A. Marangoni, C.B. Hanna, D.A. Pink, Aggregation in complex triacylglycerol oils: coarse-grained models, nanophase separation, and predicted X-ray intensities, *J. Phys. Condens. Matter* 26 (2014) 464108.
- [41] K. Kyriakos, M. Philipp, J. Adelsberger, S. Jaksch, A.V. Berezkin, D.M. Lugo, W. Richtering, I. Grillo, A. Miasnikova, A. Laschewsky, P. Müller-Buschbaum, C.M. Papadakis, Consolvency of water/methanol mixtures for PNIPAM and PS-b-PNIPAM: pathway of aggregate formation investigated using time-resolved SANS, *Macromolecules* 47 (2014) 6867–6879.
- [42] F. Peyronel, D.A. Pink, A.G. Marangoni, Triglyceride nanocrystal aggregation into polycrystalline colloidal networks: ultra-small angle X-ray scattering, models and computer simulation, *Curr. Opin. Colloid Interface Sci.* 19 (2014) 459–470.
- [43] S. Alexander, T. Cosgrove, W.M. de Vos, T.C. Castle, S.W. Prescott, Aggregation behavior of polyisoprene–pluronic graft copolymers in selective solvents, *Langmuir* 30 (2014) 5747–5754.
- [44] S. Chaieb, Elasto-plasticity in wrinkled polymerized lipid membranes, *Sci Rep* 4 (3699) (2013) 1–5.
- [45] M. Shao, J. Keum, J. Chen, Y. He, W. Chen, J.F. Browning, J. Jakowski, B.G. Sumpter, I.N. Ivanov, Y.-Z. Ma, C.M. Rouleau, S.C. Smith, D.B. Geoghan, K. Hong, K. Xiao, The isotopic effects of deuteration on optoelectronic properties of conducting polymers, *Nat. Commun.* 5 (4180) (2013) 1–11.
- [46] J.-B. Guilbaud, C. Rochas, A.F. Miller, A. Saiani, Effect of enzyme concentration of the morphology and properties of enzymatically triggered peptide hydrogels, *Biomacromolecules* 14 (2013) 1403–1411.
- [47] J.K. Keum, K. Xiao, I.N. Ivanov, K. Hong, J.F. Browning, Gregory S. Smith, Ming Shao, Kenneth C. Littrell, Adam J. Rondinone, E. Andrew Payzant, Jihua Chen, Dale K. Hensley, Solvent quality-induced nucleation and growth of parallel-epitaxial nanorods in dilute poly(3-hexylthiophene) (P3HT) solution and the impact on the crystalline morphology of solution-cast thin film, *CrystEngComm* 15 (2013) 1114–1124.

- [48] B.C. Kumi, S.C. Greer, Micelles of polybutadiene-*b*-poly(ethylene oxide) in deuterated methanol and deuterated cyclohexane, *J. Colloid Interface Sci.* 386 (2012) 212–217.
- [49] M.J. Sobkowitz, R.L. Jones, R.J. Kline, D.M. DeLongchamp, Effect of fullerenes on crystallization-induced aggregation in polymer photovoltaics casting solutions, *Macromolecules* 45 (2012) 1046–1055.
- [50] M. Singh, A.K. Singh, R.K. Mandal, I. Sinha, Synthesis of anisotropic silver nanostructures in presence of polyvinyl pyrrolidone (PVP): LSPR and SAXS analysis, *Colloids Surf. A Physicochem. Eng. Asp.* 390 (2011) 167–172.
- [51] A. Wacha, Z. Varga, U. Vainio, A. Hoell, A. Bota, Small-angle X-ray scattering experiments and computer simulations to characterise anisotropy of activated carbons prepared from wood, *Carbon* 49 (2011) 3958–3971.
- [52] M. Singh, I. Sinha, A.K. Singh, R.K. Mandal, S.A.X.S. Correlating, analysis with LSPR behavior: poly(vinyl alcohol)-stabilized Ag nanoparticles, *J. Nanopart. Res.* 13 (2011) 4387–4394.
- [53] M. Singh, I. Sinha, A.K. Singh, R.K. Mandal, LSPR and SAXS studies of starch stabilized Ag–Cu alloy nanoparticles, *Colloids Surf. A Physicochem. Eng. Asp.* 384 (2011) 668–674.